ISSN 0021-3640, JETP Letters, 2018, Vol. 107, No. 3, pp. 157–162. © Pleiades Publishing, Inc., 2018.
Original Russian Text © A.V. Orlov, M.Yu. Brazhnikov, A.A. Levchenko, 2018, published in Pis'ma v Zhurnal Eksperimental'noi i Teoreticheskoi Fiziki, 2018, Vol. 107, No. 3, pp. 166–171.

PLASMA, HYDRO- AND GAS DYNAMICS

Large-Scale Coherent Vortex Formation in Two-Dimensional Turbulence[1]

A. V. Orlov[a, b, c, *], M. Yu. Brazhnikov[a, b], and A. A. Levchenko[a, b]

[a] *Institute of Solid State Physics, Russian Academy of Sciences, Chernogolovka, Moscow region, 142432 Russia*
[b] *Landau Institute for Theoretical Physics, Russian Academy of Sciences, Moscow, 119334 Russia*
[c] *Moscow Institute of Physics and Technology (State University), Dolgoprudny, Moscow region, 141700 Russia*
**e-mail: arturor@issp.ac.ru*

Received November 2, 2017; in final form, December 4, 2017

The evolution of a vortex flow excited by an electromagnetic technique in a thin layer of a conducting liquid was studied experimentally. Small-scale vortices, excited at the pumping scale, merge with time due to the nonlinear interaction and produce large-scale structures—the inverse energy cascade is formed. The dependence of the energy spectrum in the developed inverse cascade is well described by the Kraichnan law $k^{-5/3}$. At large scales, the inverse cascade is limited by cell sizes, and a large-scale coherent vortex flow is formed, which occupies almost the entire area of the experimental cell. The radial profile of the azimuthal velocity of the coherent vortex immediately after the pumping was switched off has been established for the first time. Inside the vortex core, the azimuthal velocity grows linearly along a radius and reaches a constant value outside the core, which agrees well with the theoretical prediction.

DOI: 10.1134/S0021364018030128

INTRODUCTION

One of the key problems in turbulence is to understand processes associated with the nature of the mean (coherent) flows. The understanding of how such structures are arranged and how they interact with the flow fluctuations is important for solving many problems in a number of areas—plasma physics, atmospheric physics, geophysics, astrophysics and others. Coherent structures could be generated by both external forces and internal processes in a turbulent system, for example, due to spectral condensation in the inverse cascade [1, 2].

In this article, we study two-dimensional turbulence in a thin liquid layer when a vertical velocity component can be neglected in comparison with velocity components in the horizontal plane. The theory of two-dimensional turbulence predicts a possibility of two cascades existence: a direct cascade with a power-law dependence of the energy on the wavenumber $E(k) \propto k^{-3}$ at large wavenumbers k, greater than the characteristic pumping wavenumber k_f, and an inverse cascade directed towards smaller k, with the Kraichnan energy spectrum $E(k) = C\epsilon^{2/3}k^{-5/3}$, where C is the Kolmogorov constant, and ϵ is the energy flux in the inverse cascade [3–5]. Most of the energy injected into the system is carried by the inverse cascade and dissipates at large scales for which energy losses due to bottom friction are significant. In an infinite medium, the inverse cascade is limited by the flow scale $L_\alpha \sim \epsilon^{1/2}\alpha^{-3/2}$, where α is a bottom friction coefficient [3–5]. In a limited system, the maximum flow scale cannot be greater than the system size L. If the system size is less than the scale L_α, the spectral condensation of energy occurs in such a system—the energy carried by the inverse cascade accumulates at the scales of the order L, that results in the coherent structures formation [3]. Such structures have been observed in the experiment [6] for the first time.

At present, these structures are being actively investigated experimentally, theoretically and in numerical simulations. In the experimental work [7], the authors study coherent vortices in two-dimensional turbulence excited by the Lorentz force in a thin liquid layer. The processes of the inverse energy cascade formation and the large-scale coherent vortices formation in turbulence excited by Faraday waves are studied experimentally in the works [8, 9]. Paper [10] is devoted to theoretical studies of the coherent flow characteristics dependence on experimentally adjustable parameters. Coherent vortices also in the rectangular geometry were observed in the numerical work [11]. The radial profile of the azimuthal velocity of the coherent vortex was predicted in the theoretical and numerical researches [12–14], and in our work, the

[1] The article was translated by A.V. Orlov.

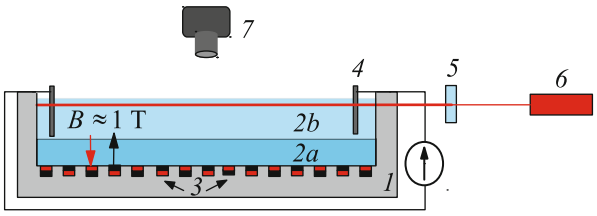

Fig. 1. (Color online) Layout of the experimental setup: (*1*) acrylic cell, (*2a*) perfluorodecalin, (*2b*) electrolyte, (*3*) magnets array, (*4*) platinum electrodes connected to the power supply, (*5*) cylindrical lens, (*6*) laser, and (*7*) video camera.

radial profile has been established experimentally for the first time.

In the case of a thin liquid layer, the bottom friction coefficient is determined by the expression $\alpha = \pi^2\nu/(4h^2)$, where ν is the kinematic liquid viscosity and h is the layer depth. To reduce the bottom friction, one can increase the liquid layer depth, but then a condition of flow two-dimensionality $h \ll L$ would be deteriorated. The use of two-layer liquids permits us to avoid this disadvantage: turbulence is excited in the upper layer, and the lower layer plays the role of a lubricant. The friction coefficient in this case can be found by determining the smallest root of the equation

$$\frac{\rho_b}{\rho}\sqrt{\frac{\nu_b}{\nu}} = \tan\left(\sqrt{\frac{\alpha}{\nu_b}}h_b\right)\tan\left(\sqrt{\frac{\alpha}{\nu}}h\right), \qquad (1)$$

where h, ν, and ρ are the depth, kinematic viscosity and density of the upper layer, respectively, and h_b, ν_b, and ρ_b are the corresponding characteristics of the lower layer.

EXPERIMENTAL TECHNIQUE

The layout of the experimental setup is shown in Fig. 1. The measurements were carried out in a 10 × 10 × 1.5-cm acrylic glass cell. A layer of perfluorodecalin (the depth was $h_b = 0.45$ cm), an insoluble non-conductive liquid, was poured onto the cell bottom. The density of perfluorodecalin is $\rho_b = 1.95$ g/cm^3, the kinematic viscosity is $\nu_b = 2.7 \times 10^{-2}$ cm^2/s. A layer of an electrolyte (the depth was $h = 0.85$ cm), a 20-percent solution of KNO_3 in distilled water, was poured over perfluorodecalin. The electrolyte density is $\rho = 1.15$ g/cm^3, the viscosity of the electrolyte slightly depends on the salt concentration and is close to the water viscosity $\nu \approx 10^{-2}$ cm^2/s. A chess-like 10 × 10 array of cylindrical magnets was mounted below the cell bottom, so the fields of two nearest magnets were directed in opposite sides. A distance between the nearest magnets centers was 1 cm. A value of a non-uniform **B**-field near a surface of the magnets was ≈1 T. Platinum electrodes, immersed into the electrolyte, were connected to a DC power supply. When a current $I = 6.4$ A was passed through the electrolyte, the fluid was driven by the Lorentz force (Fig. 2).

Electrolyte flows were detected by the PIV (particle image velocimetry) technique. A polyamide powder with the average particle diameter of ≈30 μm was poured to the liquid. The density of polyamide particles is close to the density of the electrolyte, the particles are localized under the surface in small aggregates-tracers with the average sizes of ≈200 μm and are completely carried away by fluid motions. To detect the motions of polyamide tracers only in a thin layer near the surface, the liquid surface was illuminated by

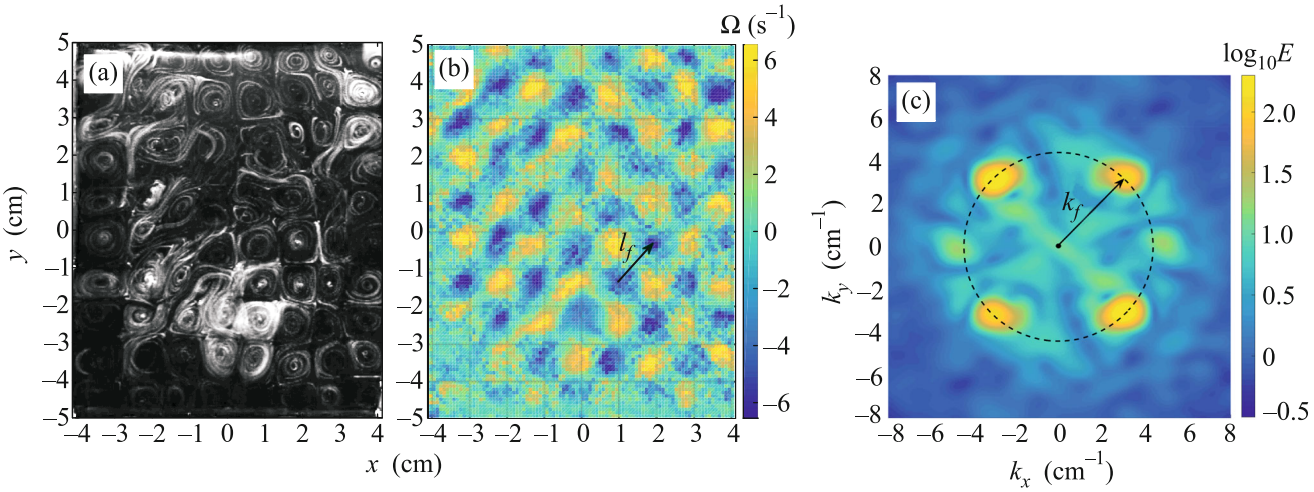

Fig. 2. (Color online) (a) Polyamide tracers tracks on the electrolyte surface. (b) Vorticity distribution $\Omega(x, y)$ on the electrolyte surface, the pumping scale $l_f \approx \sqrt{2}$ cm. (c) Energy distribution by the wavenumbers $E(k_x, k_y)$ at the logarithmic scale in 3 s after the pumping was switched on. The pumping wavenumber $k_f \approx 4.4$ cm^{-1}.

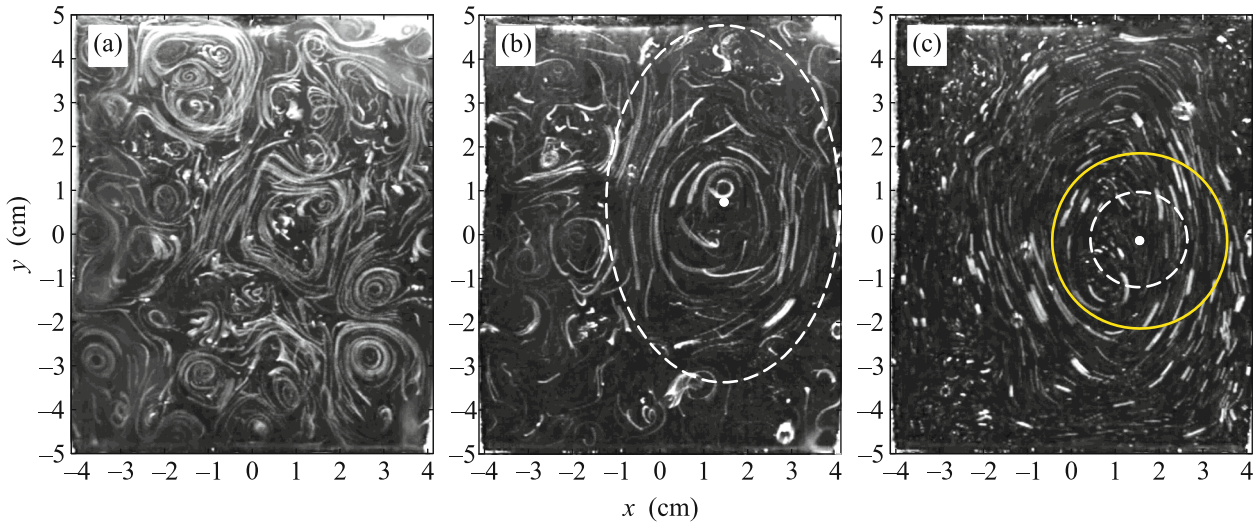

Fig. 3. (Color online) Polyamide tracers tracks on the electrolyte surface: (a) 1 min after the pumping was switched on and (b) in 5 min. The approximate boundaries of the large-scale flow are indicated by the ellipse. (c) Polyamide tracers tracks in 13 seconds after the pumping was switched off. The radii of the outer and inner circumferences are ≈2 and 0.9 cm, respectively. The instant positions of the coherent vortex center are indicated by the white small circles.

a laser sheet with a thickness of ≈1 mm. The sheet was formed when a laser beam passed through a cylindrical lens. The motion of the illuminated tracers was registered by the Canon EOS 6D camera with a rate of 24 frames per second. To obtain the tracers tracks, the frames were superimposed on each other and then averaged (Figs. 2a and 3). The processing of the obtained frames by the PIVLab program [15] made it possible to calculate the velocity components of the tracers $v_x(x, y)$ and $v_y(x, y)$, and to calculate a vorticity on the liquid surface, which is defined by the expression

$$\Omega(x, y) = \frac{\partial v_x}{\partial y} - \frac{\partial v_y}{\partial x}. \quad (2)$$

The distribution of the energy per unit mass by wavenumbers $E(k_x, k_y)$ can be calculated using the known values v_x and v_y as a discrete spatial Fourier transform of the kinetic energy of the two-dimensional system. An energy distribution by the absolute value of the wavenumber (energy spectrum) can be calculated by averaging $E(k_x, k_y)$ over a ring in the (k_x, k_y)-space:

$$E(k) = \frac{1}{2S\Delta k}\int \frac{d^2q}{(2\pi)^2}\left\lfloor |\mathbf{v_q}|^2 \right\rfloor. \quad (3)$$

The integration is carried out in the ring $k < q < k + \Delta k$. The resulting value of the integral is normalized by the surface area of the liquid S. Here, $\mathbf{v_q}$ is a Fourier component of velocity on the liquid surface. Brackets $\lfloor\ \rfloor$ mean averaging over 24 consecutive frames.

During the experiment, when the current was being passed through the electrolyte, the gas bubbles were being formed on the electrodes and this made it difficult to detect the flows. Therefore, the polymeric small curtains were installed near the electrodes, thus the observation field was limited in size by $L_x \times L_y = 8.25 \times 10$ cm.

EXPERIMENTAL RESULTS AND DISCUSSIONS

Figure 2a shows the tracks of polyamide tracers on the electrolyte surface after 3 s of pumping. One can clearly see an 8 × 10 vortex lattice with a diameter of ≈1 cm. Figure 2b shows the vorticity distribution $\Omega(x, y)$ calculated by Eq. (2). It can be seen that the nearest neighbors in the lattice rotate in the opposite directions, thus, the vortices form a chess-like structure. Figure 2c explains a value of the pumping scale l_f, it shows the energy distribution $E(k_x, k_y)$ after 3 s of pumping. This allows one to determine on which wavenumbers (spatial scales) a certain amount of energy is concentrated. One can clearly see four peaks with approximately equal amplitudes at a distance $k_f \approx 4.4\ \text{cm}^{-1}$ from origin in [11] and [−11] directions—directions of the symmetry of vortices with the same vorticity sign, which coincides with the symmetry of the magnets subarray with the same orientation of poles with a period of $\sqrt{2}$ cm. These peaks refer to the lattice of vortices excited at the pumping scale. The values of the pumping scale and the pumping wavenumber are related by the expression $l_f = 2\pi/k_f \approx 1.4$ cm. The mean fluid velocity in the area between

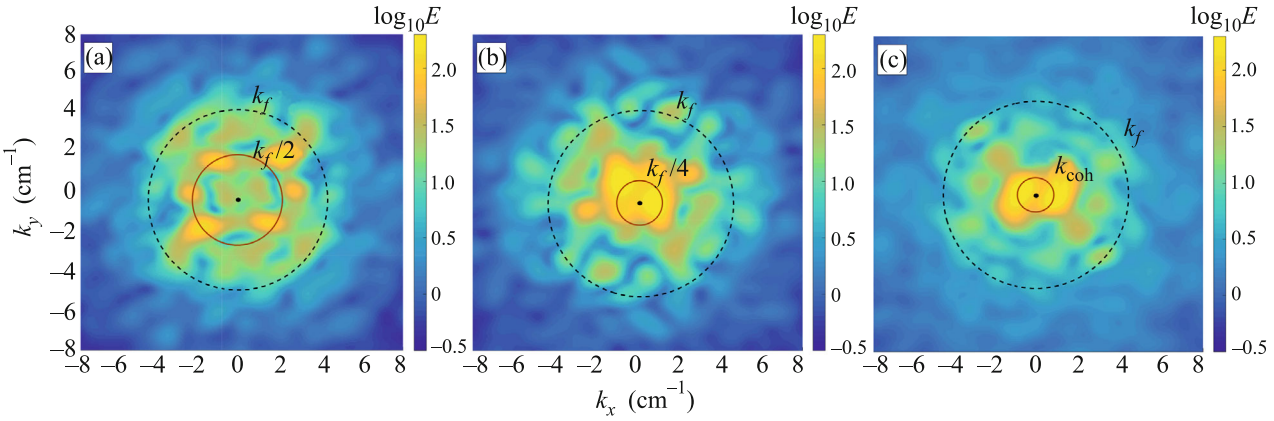

Fig. 4. (Color online) Energy distribution by the wavenumbers $E(k_x, k_y)$ at the logarithmic scale: (a) in 5 s after the pumping was switched on, (b) in 1 min, (c) in 5 min. The pumping wavenumber $k_f \approx 4.4$ cm^{-1}, the wavenumber of the coherent vortex $k_{\text{coh}} \approx 0.85$ cm^{-1}.

the vortices, determined by the PIV algorithm, is $v_f \approx 2$ cm/s. The Reynolds number at this scale is $\text{Re}_f = v_f l_f/\nu \approx 280 \gg 1$. After 3 s of pumping when the lattice was formed, the vortices begin to nonlinearly interact with each other and merge forming larger-scale structures. The characteristic vortices scale increases approximately twice between the third (see Fig. 2) and the fifth seconds, and then between the fifth second and the first minute (see Fig. 3a). In Fig. 3b, the largest-scale vortex in the system, the approximate boundaries of which are indicated by a white dashed ellipse, could be seen. After 5 min of pumping, a characteristic size of the vortex is close to the cell sizes. The evolution of the maximum vortex scale can be seen in Fig. 4, which shows the energy distribution $E(k_x, k_y)$ by the wavenumbers. The dashed circle has a radius k_f and a center at origin. One can see that most of the system energy after 5 s of pumping (see Fig. 4a) is placed at a distance $k \approx k_f/2$ from origin and concentrated in vortices with characteristic spatial scales twice as large as l_f. After 1 min (Fig. 4b), most of the system energy is concentrated in vortices with the characteristic size four times larger than l_f, and after 5 min (Fig. 4c) – in the vortex with a wavenumber $k_{\text{coh}} \approx 0.85$ cm^{-1}, i.e., in the vortex with characteristic size $L_{\text{coh}} \approx 7.5$ cm.

Figure 5 shows the energy spectra calculated in accordance with the formula (3). From the beginning, the most part of the energy coming into the system is focused on $k_f \approx 4.4$ cm^{-1} (the curve *a* is the spectrum after 1 s of pumping, multiplied by 10, the other curves are not multiplied). Then, after 5 s of pumping (curve *b*) there is a peak at $k \approx 2.2$ cm^{-1} (at large spatial scales). It contains more energy than the peak at the pumping wavenumber, i.e., the energy is carried to smaller k by the (undeveloped) inverse cascade. After 1 min of pumping (curve *c*), a peak at $k \approx 1.1$ cm^{-1} is observed, the dependence of the energy spectrum on the wavenumber in a range from k_f to this peak (the inertial interval) is close to the theoretically predicted $E(k) \propto k^{-5/3}$ [3–5]. For comparison, a dotted line corresponding to the law $k^{-5/3}$ is shown in Fig. 5. After 5 min of pumping (curve *d*), a developed inverse cascade in the inertial interval is observed, and the energy dependence on the wavenumber is close to predicated by the theory $E(k) \propto k^{-5/3}$. A peak at $k_{\text{coh}} \approx 0.85$ cm^{-1} corresponds to the vortex with diameter $L_{\text{coh}} \approx 7.5$ cm. The velocity at the periphery of this vortex (see Fig. 3b) determined by the PIV algorithm is $v_{\text{coh}} \approx 1.7$ cm/s. The vortex center, defined as a region with the maximum absolute value of vorticity, is shown in the figure by a white small circle. The Reynolds number is $\text{Re}_{\text{coh}} = v_{\text{coh}} L_{\text{coh}}/\nu \approx 1300$.

The value of the energy flux in the inverse cascade ϵ can be found from the energy balance in the quasi-stationary mode, when the system energy varies slightly with time. In this case, the energy flux is approximately equal to the energy dissipated per unit time: $\epsilon \approx \int_{k_{\text{coh}}}^{k_f} (\gamma_k + 2\alpha) E(k) dk$, where $\gamma_k = 2\nu k^2$ is the coefficient of the energy damping due to the bulk viscosity. The value of the cell bottom friction coefficient, estimated by the expression (1) $\alpha \approx 2.3 \times 10^{-2}$ s^{-1}, agrees with the experimental value obtained from observing the final stage of relaxation of the large-scale flow. Using the spectrum $E(k)$ obtained from the experimental data the energy flux is evaluated to be $\epsilon = (3 \pm 1) \times 10^{-2}$ cm^2/s^3. Now one can estimate that the spatial scale, at which the inverse cascade must break in an infinite system $L_\alpha \sim \epsilon^{1/2} \alpha^{-3/2} \approx 50$ cm, is much larger than the cell size $L = 10$ cm.

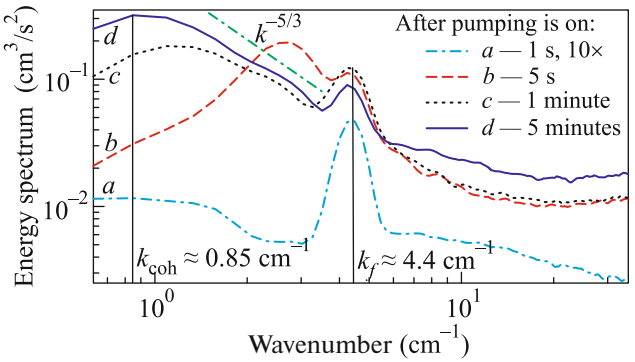

Fig. 5. (Color online) Energy spectrum at the log-log scale at different times after the pumping was switched on: (*a*) in 1 s (the spectrum is multiplied by 10 for convenience of the comparison), (*b*) 5 s, (*c*) 1 min, and (*d*) 5 min.

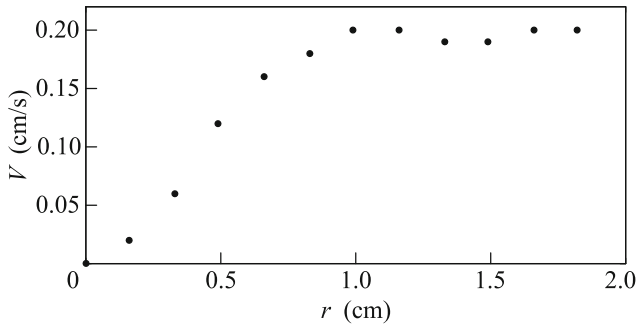

Fig. 6. Radial profile of the azimuthal velocity in the outer circle in Fig. 3c in 13 s after the pumping was switched off.

In Fig. 3b, one can see strong fluctuations from small-scale vortices, especially from vortices at the pumping scale. To reduce their influence, one could switch off the pumping. The small-scale vortices, connected mainly with the lattice and large k, would quickly decay owing to the large coefficient of energy damping due to the bulk viscosity and one will be able to observe a coherent vortex without significant fluctuations and to study its structure. Indeed, for $k \geq k_f$ where the conditions $\gamma_k \geq \gamma_{k_f} \approx 0.4$ s^{-1} are satisfied, the coefficient γ_k is much larger than the energy damping coefficient equal to $2\alpha \approx 0.05$ s^{-1} at small k.

Figure 3c shows polyamide tracers tracks on the electrolyte surface at the moment 13 s after the pumping was switched off. The coherent vortex in Fig. 3c drifts with a characteristic velocity of the center $V_{dr} \approx 0.2$ cm/s. In order to study the velocity distribution in the vortex, it is more convenient to pass to the frame of reference connected with the vortex center. The vortex center was determined by the maximum of the absolute value of vorticity. Figure 6 shows the radial profile of the azimuthal velocity in the vortex center frame in 13 s after the pumping was switched off in a circle bounded by the outer circumference in Fig. 3c with a radius of ≈2 cm. It is seen that inside the vortex core, in a circle with a radius $r_c \approx 0.9$ cm, bounded by the inner circumference in Fig. 3c, a linear dependence of the coherent vortex azimuthal velocity on the radius is observed. Then, the velocity goes to the plateau at the level $V \approx 0.2$ cm/s.

As it was established theoretically in [12], in a cell with periodic boundary conditions and under a short correlated in time pumping, the azimuthal velocity of the coherent vortex does not depend on a distance from the vortex center $V \sim \sqrt{3\epsilon/\alpha}$. In this work, a computer simulation was also carried out, the results of which are in a good agreement with theoretical predictions. In subsequent works [13, 14], the theory was developed further and it was found that in the vortex core near the vortex center the azimuthal velocity grows linearly along the radius. It was established that the core radius $r_c \sim \sqrt{\nu/\alpha}$.

In this paper, the pumping is static, the boundary conditions are zero (flow velocities near the cell boundaries are zero). However, one can use the results of the presented theory to make estimations. In accordance with the theoretical predictions, when the pumping is switched on, the core radius should reach $r_c \sim \sqrt{\nu/\alpha} \approx 0.7$ cm, the azimuthal velocity on the plateau $V \sim \sqrt{3\epsilon/\alpha} = (2.0 \pm 0.5)$ cm/s. From the energy distribution in Figs. 4c and 5 (curve *d*) it follows that most of the system energy is concentrated in the coherent vortex. Then, the total energy of flows on the electrolyte surface per unit mass in t seconds after the pumping was switched off can be estimated as: $E_{tot}(t) \approx V_{coh}^2(t)/2$, where $V_{coh}(t)$ is a characteristic velocity of the coherent vortex at the time t after the pumping was switched off. Consequently, $V_{coh}(13) \approx \sqrt{E_{tot}(13)/E_{tot}(0)}V \approx 0.45$ cm/s, where $E_{tot}(0) \approx 2 \times 10^{-2}$ cm^2/s^2 and $E_{tot}(13) \approx 1 \times 10^{-3}$ cm^2/s^2 are the experimental values of the total energy per unit mass just before the pumping was switched off and 13 s after switching off, respectively. In the vortex center frame, which is drifting at a rate $V_{dr} \approx 0.2$ cm/s, the azimuthal velocity outside the core in 13 s after the pumping was switched off can be estimated as: $V \approx V_{coh}(13) - V_{dr} = (0.25 \pm 0.07)$ cm/s, which is close to the experimentally observed value.

CONCLUSIONS

In this paper, the process of the inverse energy cascade formation in the two-dimensional system is studied. It is found that the observed dependence of the energy on the wavenumber is close to predicted by the theory $E(k) \propto k^{-5/3}$ [3–5]. It is shown that small-scale vortices, initially excited at the pumping scale in a thin liquid layer, merge due to the nonlinear interaction

and form large-scale flows. The bottom friction and the pumping power were at such level that the maximum vortex scale was limited only by the cell sizes. The energy carried to this scale by the inverse cascade was accumulated in the vortex, which permitted us to observe spectral condensation and formation of the coherent vortex. However, at the same time there were strong fluctuations from small-scale vortices in the system. After switching off the pumping, they quickly decay, and due to this in 13 s one could observe a coherent vortex with the size close to the system size, and could study the vortex structure. The radial profile of the azimuthal velocity of the coherent vortex in the frame of its drifting center after the pumping was switched off has been established for the first time. It turned out that inside the vortex core the azimuthal velocity grows linearly, and the azimuthal velocity outside the core is close to a constant. The results of these studies are in a good agreement with theoretical predictions [12–14].

We are grateful to V.V. Lebedev, I.V. Kolokolov, L.P. Mezhov-Deglin, and V.M. Parfenyev for valuable discussions and to S.V. Filatov for assistance in the experimental data processing by the PIVlab program. The work was supported by the Russian Science Foundation, project no. 14-22-00259.

REFERENCES

1. G. Boffetta and R. E. Ecke, Ann. Rev. Fluid Mech. **71**, 427 (2012).
2. L. M. Smith and V. Yakhot, Phys. Rev. Lett. **71**, 352 (1993).
3. R. H. Kraichnan, Phys. Fluids **10**, 1417 (1967).
4. C. E. Leith, Phys. Fluids **11**, 671 (1968).
5. G. K. Batchelor, Phys. Fluids **12**, 233 (1969).
6. J. Sommeria, J. Fluid Mech. **170**, 139 (1986).
7. H. Xia, M. Shats, and G. Falkovich, Phys. Fluids **21**, 125101 (2009).
8. N. Francois, H. Xia, H. Punzmann, and M. Shats, Phys. Rev. Lett. **110**, 194501 (2013).
9. N. Francois, H. Xia, H. Punzmann, S. Ramsden, and M. Shats, Phys. Rev. X **4**, 021021 (2014).
10. I. V. Kolokolov and V. V. Lebedev, JETP Lett. **106**, 659 (2017).
11. A. Frishman, J. Laurie, and G. Falkovich, Phys. Rev. Fluids **2**, 032602 (2017).
12. J. Laurie, G. Boffetta, G. Falkovich, I. Kolokolov, and V. Lebedev, Phys. Rev. Lett. **113**, 254503 (2014).
13. I. V. Kolokolov and V. V. Lebedev, Phys. Rev. E **93**, 033104 (2016).
14. I. V. Kolokolov and V. V. Lebedev, J. Fluid Mech. **809**, R2-1 (2016).
15. W. Thieckle and E. J. Stamhuis, J. Open Res. Software **2**, 30 (2014).